

EAN-MapNet: Efficient Vectorized HD Map Construction with Anchor Neighborhoods

Huiyuan Xiong^{1,2} Jun Shen^{1,2} Taohong Zhu^{1,2} Yuelong Pan^{3,4 *}

¹ School of Intelligent Systems Engineering, Sun Yat-sen University
 {shenj57, zhuth3}@mail2.sysu.edu.cn
 xionghy@mail.sysu.edu.cn

² Guangdong Provincial Key Laboratory of Intelligent Transport System
³ China Nuclear Power Design Co.,Ltd.
 panyuelong@cgnpc.com.cn

⁴ State Key Laboratory of Nuclear Power Safety Technology and Equipment, China
 Nuclear Power Engineering Co., Ltd., Shenzhen, Guangdong, 518172, China

Abstract. High-definition (HD) map is crucial for autonomous driving systems. Most existing works design map elements detection heads based on the DETR decoder. However, the initial queries lack integration with the physical location feature of map elements, and vanilla self-attention entails high computational complexity. Therefore, we propose **EAN-MapNet** for Efficiently constructing HD map using Anchor Neighborhoods. Firstly, we design query units based on the physical location feature of anchor neighborhoods. Non-neighborhood central anchors effectively assist the neighborhood central anchors in fitting to the target points, significantly improving the prediction accuracy. Then, we introduce grouped local self-attention (GL-SA), which innovatively utilizes local queries as the medium for feature interaction, thereby substantially reducing the computational complexity of self-attention while facilitating ample feature interaction among queries. On nuScenes dataset, EAN-MapNet achieves a state-of-the-art performance with 63.0 mAP after training for 24 epochs. Furthermore, it considerably reduces memory consumption by 8198M compared to the baseline.

Keywords: HD map, neighborhoods, grouped local self-attention, local queries

1 Introduction

In autonomous driving systems, HD map leverage rich semantic information, accurately reflecting the road environment, and providing robust data support for planning and decision-making [1–3]. However, the traditional creation process of HD map begins with capturing point clouds and constructing map through SLAM [4–6]. Subsequently, it heavily relies on a large amount of human resources for annotation and maintenance. Consequently, it faces challenges such as high construction costs, poor scalability, and low data freshness.

* Corresponding author.

In recent years, the researchs on end-to-end HD map generation networks have gained significant attention. Early works focused on semantic segmentation of bird's eye view (BEV) to identify map elements pixel by pixel [7–9]. However, It is evident that these works require intricate post-processing steps to generate the vectorized representation of map elements. Therefore, the approaches of representing map elements as sequences of points have been introduced [10–14]. Typically, such methods design detection heads based on the structure of the DETR decoder [15]. The initial queries, after feature aggregation, undergo MLP to output the category and coordinates of the points.

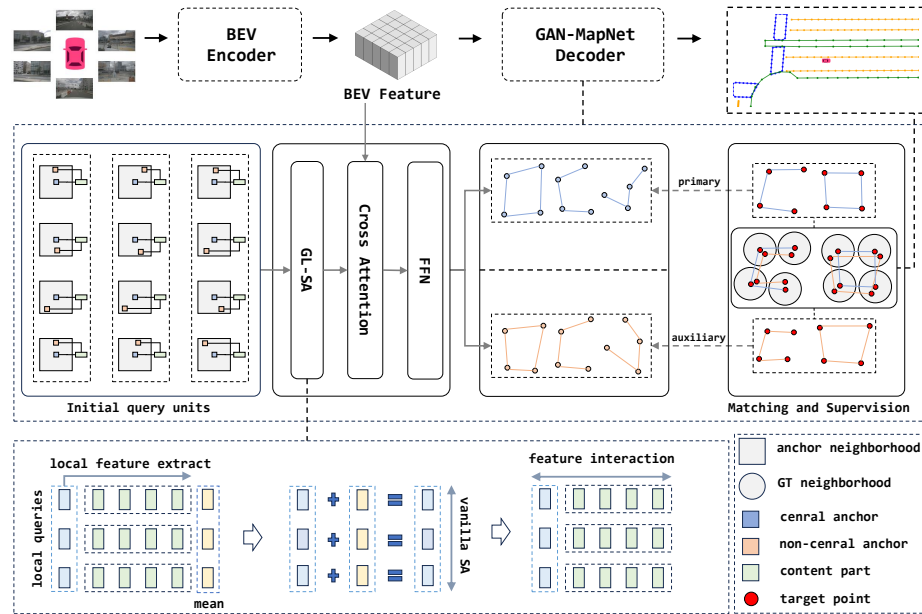


Fig. 1: The overall architecture of EAN-MapNet: First, images captured by the surround-view cameras undergo transformation into unified BEV feature by the BEV Encoder. Then, GAN-MapNet's decoder continuously updates anchors based on input anchor query units and BEV feature, finally obtaining the HD map.

However, these type of networks structure have the following two drawbacks: One drawback is the design of queries neglects the incorporation of positional feature of map elements. In the deformable attention [16], the coordinates of the initial reference points are predicted by MLP from n -dimensional positional queries. However, since the positional queries are unrelated to BEV, it restricts the networks' comprehension of positional prior information. Another drawback is the high computational complexity of vanilla self-attention, making it difficult

to meet the demand for setting a large number of queries to enhance model prediction diversity. Furthermore, vanilla self-attention overlooks the strong correlation among queries within the same instance.

Therefore, we propose EAN-MapNet, whose overall structure is illustrated in [Fig\(1\)](#). We similarly represent map elements as sequences of points and then randomly initialize a certain number of anchors. EAN-MapNet formulates the task of detecting map elements as the process of fitting initial anchors to target points.

To effectively leverage the physical location feature of anchors, we define a neighborhood around each anchor with a certain size, and then each neighborhood corresponds to a query unit. As illustrated in [Fig\(2\)](#). A query unit consists of a neighborhood central query and a non-neighborhood central query, each comprising positional and content part. Non-neighborhood central anchors and neighborhood central anchors exhibit strong correlations in terms of positional prior information. Additionally, during training, we allow them to share content parts. Consequently, non-neighborhood central anchors can effectively assist neighborhood central anchors in fitting to target points. Note that neighborhood central anchors are fitted to target points, while non-neighborhood central anchors are fitted to random points within the GT neighborhood, thereby avoiding fitting ambiguities. Additionally, the non-neighborhood central anchor queries are exclusively involved in the network training process and do not consume computational resources required for network inference.

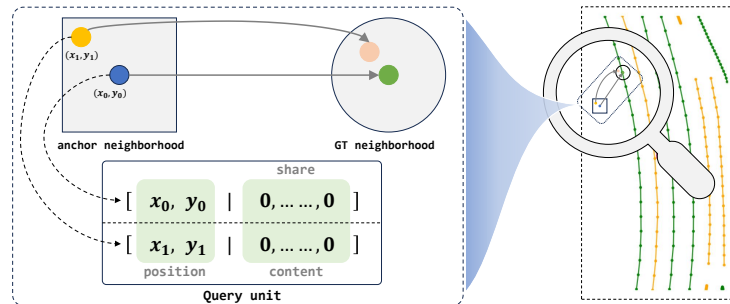


[Fig. 2](#): A single query unit corresponds to two queries, each composed of the 2-dimensional coordinates of anchors situated in the initial neighborhood, along with shared n -dimensional learnable parameters. The neighborhood central anchor is fitted to the target point, whereas the non-neighborhood central anchor is fitted to random point within the ground truth(GT) neighborhood.

The queries within the same group represent vertices of the same map elements, exhibiting strong feature correlation among them, while the relative positions between different map elements are also crucial feature. So, we propose GL-SA, where each query interacts only with other queries within the same

group, while interactions with queries from different groups are mediated by local queries. In contrast, in vanilla self-attention, each query interacts with all other queries. Therefore, GL-SA enhances feature interaction within the same group of queries while efficiently facilitating feature interaction among queries from different groups.

The contributions of this paper are as follows:

- We formulate query units that incorporate the physical location feature of the anchor neighborhoods, leveraging non-neighborhood central anchors to effectively assist in fitting the neighborhood central anchors to the target points.
- We propose GL-SA, which enhances feature interaction among queries within the same group and efficiently facilitates feature interaction among queries from different groups.
- We validate the effectiveness of the proposed design methodology on the nuScenes dataset and achieve a prediction accuracy of 63.0 mAP after training for 24 epochs, outperforming existing state-of-the-art approaches.

2 Related works

2.1 DETR

We refer to the structure of the DETR decoder for the design of the map elements detection heads. However, DETR suffers from slow convergence, prompting numerous approaches to address this issue. Deformable DETR [16] introduces deformable attention. each query is updated based on information extracted from sampled points on the feature maps output by the decoder. DN-DETR [17] and DION [18] incorporate a denoising part into network training. This part takes labels with randomly added noise as input, and its output is directly supervised by GT labels without requiring Hungarian matching, thus mitigating the ambiguity caused by unstable matching. The inspiration for the neighborhood concept in EAN-MapNet is derived from the denoising part. Anchor DETR [19], Conditional DETR [20], and DAB-DETR [21] initialize queries based on anchor coordinates, thereby providing them with explicit physical meaning. However, anchor queries only focus on the position information of the anchors themselves, neglecting the positional feature of the surrounding anchor regions. Therefore, we design query units based on anchor neighborhoods.

2.2 Self-attention

In vanilla self-attention [22], each query interacts with all other queries. To improve computational efficiency, multi-query attention [23] proposes sharing keys and values among all queries. However, this approach may result in a degradation in the quality of feature interaction. Therefore, grouped-query attention [24] divides queries into groups, where queries within the same group share keys and

values. Additionally, in long sequence time-series forecasting, due to the sparsity of self-attention, Informer [25] introduces probssparse self-attention, which filters queries based on their sparsity measure to reduce computational complexity. These self-attention mechanisms struggle to integrate feature related to the relative positional relationships between queries. Hence, we introduce GL-SA. GL-SA strengthens feature interaction among queries within the same group and achieves interactions among queries from different groups using local queries.

2.3 Representation of map elements

To achieve end-to-end HD map construction, the first step is to determine the representation of map elements. The pixel-based representation methods [7, 8, 26, 27] rasterize map elements into pixels and perform pixel-level classification on the BEV to identify the positions of map elements. These methods require complex post-processing to generate vectorized representation of map elements. Therefore, MapTR [10], StreamMapNet [12] and InsightMapper [13] describe map elements as equivalent point sequences. Their queries generate coordinates and categories of points representing map elements by continuously aggregating feature. However, if anchors within the same anchor neighborhoods are fitted to the same target points, ambiguities arise. Therefore, we propose reconstructing map elements based on the GT neighborhoods to obtain the fitting targets for non-neighborhood central anchors.

3 Methods

3.1 Grouped anchor query units

Firstly, we represent map elements as a collection of polylines, denoted as $V = \{V_i\}_{i=0}^M$, where M represents the number of instances of map elements. Each polyline V_i is composed of an ordered set of vertices, denoted as $V_i = \{v_j\}_{j=0}^N$, where N represents the number of vertices in each map element.

Then, we randomly initialize a group of anchors on the BEV plane, denoted as $\{p_j\}_{j=0}^N$, with coordinates $\{(x_j, y_j)\}_{j=0}^N$. Subsequently, we create a square neighborhood with side length a around each anchor and assume non-central anchors are denoted as $\{p'_j\}_{j=0}^N$.

Our goal is to fit the initial neighborhood central anchors to the vertices representing map elements. Therefore, our first step is to construct query units based on anchor neighborhoods.

Taking an anchor neighborhood U_j as an example, we construct neighborhood central anchor queries q_j and non-neighborhood central anchor queries q'_j for p_j and p'_j , respectively. q_j and q'_j together form a query unit, both of which can be decomposed into positional and content part, as shown in [Equation\(1\)](#). Here, The content part c_j is shared and represented as an n -dimensional learnable parameter responsible for generating the offset Δ_j from the anchor to the target point, along with the anchors' categorical information.

$$\begin{cases} q_j = \text{Cat}(p_j, c_j) \\ q'_j = \text{Cat}(p'_j, c_j) \end{cases} \quad (1)$$

A set of query units can only represent a single map element. To depict map elements of different instances, we introduce grouping embeddings for the positional and content parts of anchor queries, denoted as $\{g_i^p\}_{i=0}^{\hat{M}}$ and $\{g_i^c\}_{i=0}^{\hat{M}}$, where $\hat{M} \geq M$, is the number of groups. Therefore, the j -th neighborhood central anchor query q_{ij} in the i -th group is expressed as given in [Equation\(2\)](#).

$$q_{ij} = \text{Cat}(p_j + g_i^p, c_j + g_i^c) \quad (2)$$

As for the representation of non-neighborhood center anchor queries, we assume that the distance between p'_j and p_j is $(\Delta x_j, \Delta y_j)$, which can be computed using [Equation\(3\)](#).

$$\begin{cases} \Delta x_j = \beta_1 * a/2 \\ \Delta y_j = \beta_2 * a/2 \end{cases} \quad (3)$$

where β_1 and β_2 are random numbers in the interval $(-1, 1)$.

Then according to [Equation\(\(1\)–\(3\)\)](#), the j -th non-neighborhood central anchor query q'_{ij} in the i -th group can be expressed as given in [Equation\(4\)](#).

$$q'_{ij} = \text{Cat}((p_j + g_i^p) + (\Delta x_j, \Delta y_j), c_j + g_i^c) \quad (4)$$

In summary, the neighborhood central anchor queries are denoted as $Q = \{Q_i\}_{i=0}^{\hat{M}} = \left\{ \{q_{ij}\}_{j=0}^N \right\}_{i=0}^{\hat{M}}$ and the non-neighborhood central anchor queries are denoted as $Q' = \{Q'_i\}_{i=0}^{\hat{M}} = \left\{ \{q'_{ij}\}_{j=0}^N \right\}_{i=0}^{\hat{M}}$.

3.2 GT neighborhoods

Nevertheless, ambiguities may arise when both central anchors and non-central anchors are fitted to the same target points using identical content parts. To address this issue, we propose the GT neighborhoods, where non-central anchors are no longer fitted to target points but are instead fitted within the GT neighborhoods.

As depicted in [Fig\(3\)](#), we expect that the polyline V'_i reconstructed from the points within the GT neighborhoods should undergo minimal change in shape compared to V_i . Therefore, the key lies in determining the shape and size of the neighborhoods.

Since the vertices of the GT polylines are uniformly sampled and have the same number across different polylines, the distances between vertices may vary due to the different lengths of the polylines. To accommodate this, we set the neighborhood of each vertex as a circular region with a radius of r , where r is capped at half the distance between vertices.

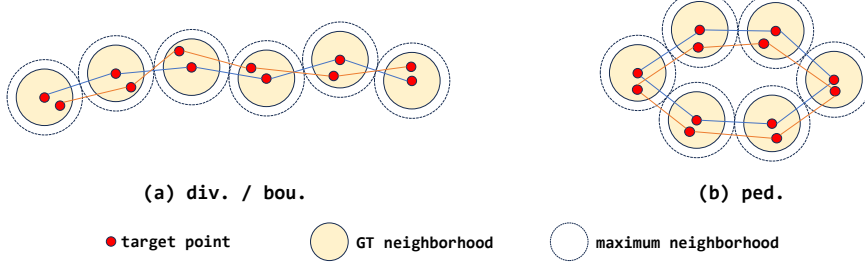


Fig. 3: GT neighborhoods: We determine the maximum radius r of the circular GT neighborhoods by half of the distance between vertices, and then further reduce the radius of the GT neighborhoods according to ω , so as to maintain the overall shape feature of the map elements to the greatest extent.

Suppose the coordinates of the vertices of the GT polyline V_i are denoted as $\{(x_j, y_j)\}_{j=0}^N$, and the distance between vertices is d . Then, the range of deviation $(\Delta x_i, \Delta y_i)$ of non-neighborhood central anchors relative to neighborhood central anchors is given by Equation(5).

$$\begin{cases} r = \omega * (d/2) \\ \Delta x_i = \beta_1 * r \\ \Delta y_i = \beta_2 * \sqrt{r^2 - \Delta x_i^2} \end{cases} \quad (5)$$

where $\omega \in (0, 1]$, β_1 and β_2 are random numbers in the interval $(-1, 1)$.

3.3 GL-SA

The pseudocode of GL-SA can be found in Alg(1). For simplicity, we analyze the implementation process and complexity of each step in the single-head GL-SA.

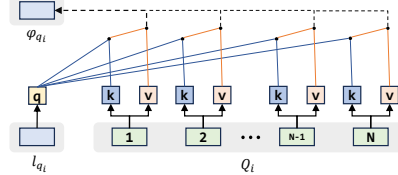


Fig. 4: Local feature extraction

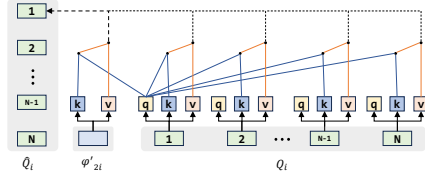


Fig. 5: Feature interaction within groups

step1:Local feature extraction. We define a set of learnable parameters $L = \{l_i\}_{i=0}^{\hat{M}}$ as local queries. The element l_i is used to query the anchor queries Q_i to obtain the local feature of the i -th group.

Due to the introduction of anchor neighborhoods, the initial queries have doubled in number. To enhance the capability of aggregating features using local queries, We partition l_i into two components, l_{q_i} and l_{p_i} , doubling the dimensionality of the local queries compared to the anchor queries. Moreover, The feature aggregation method for both l_{q_i} and l_{p_i} is consistent. Therefore, we only analyze the process of extracting local feature by l_{q_i} .

For further simplicity, we take the process of GL-SA implementing feature interaction in a group of anchor queries as an example for analysis.

As shown in [Fig\(4\)](#), Q_i generates k_{Q1_i} and v_{Q1_i} through a linear layer, while l_{q_i} generates $q_{l_{q_i}}$ through another linear layer. Assuming the embedding dimension of the queries is d , so the $q_{l_{q_i}} \in \mathbb{R}^{1*d}$, $k_{Q1_i} \in \mathbb{R}^{N*d}$ and $v_{Q1_i} \in \mathbb{R}^{N*d}$. Then, $q_{l_{q_i}}$ query k_{Q1_i} to obtain the attention matrix A_{q_i} , with the computational complexity of $A_{q_i} = q_{l_{q_i}} * k_{Q1_i}^T \in \mathbb{R}^{N*N}$ is $O(N*d)$. Subsequently, the computational complexity of $\text{softmax}(A_{q_i})$ is $O(N)$. After applying softmax, A_{q_i} is multiplied by v_{Q1_i} to obtain φ_{q_i} with a computational complexity of $O(N*d)$. Therefore, the computational complexity of Step 1 is $O_1 = O(2*N*d + N)*M$.

step2:Feature interaction among groups. Firstly, compute the mean q_m of the content part $\{C_i\}_{i=0}^{\hat{M}}$ with the added positional encoding $\text{sinPE}(\{P_i\}_{i=0}^{\hat{M}})$. Then, calculate the mean of the sum of Ψ_q and Ψ_p , and add q_m to obtain the local feature Ψ_2 . Ψ_2 is fed into vanilla self-attention to get Ψ_2' , which realizes the feature interaction among groups. Given $\Psi_2 \in \mathbb{R}^{M*d}$, the computational complexity of Step 2 is $O_2 = O(M^2*d)$.

step3:Feature interaction within groups. The elements of Ψ_2' are assigned to the initial groups, and in each group, anchor queries query all the queries including the local queries to realize the feature interaction within groups.

As shown in [Fig\(5\)](#), The keys and values generated by φ_{2_i}' and Q_i are respectively combined to obtain k_{LQ_i} and v_{LQ_i} , so $v_{LQ_i} \in \mathbb{R}^{(N+1)*d}$ and $k_{LQ_i} \in \mathbb{R}^{(N+1)*d}$. Then, q_{Q2_i} generated by Q_i query k_{LQ_i} to obtain the attention matrix A_{2_i} , with the computational complexity of $A_{2_i} = q_{Q2_i} * k_{LQ_i}^T \in \mathbb{R}^{N*(N+1)}$ is $O(N*(N+1)*d)$ in combination with $q_{Q2_i} \in \mathbb{R}^{N*d}$. Subsequently, the computational complexity of $\text{softmax}(A_{2_i})$ is $O(N)$. After applying softmax, A_{2_i} is multiplied by v_{LQ_i} to obtain \hat{Q}_i , with a computational complexity $O(N*(N+1)*d)$. Therefore, the computational complexity of Step 3 is $O_3 = O(2*N*(N+1)*d + N)*M$.

In summary, the computational complexity of GL-SA is $O_{GL} = O_1 + O_2 + O_3$. For vanilla self-attention, the computational complexity is $O_{van.} = O(((M*N)^2)*d)$.

To compare GL-SA and vanilla self-attention, we use the scaling factor ∂ , which is calculated as [Equation\(6\)](#). Therefore, the computational complexity of GL-SA is markedly reduced compared to vanilla self-attention.

$$\partial = \frac{O_{GL}}{O_{van.}} \approx \frac{2}{M} + \frac{1}{N^2} \ll 1 \quad (6)$$

In the experimental section, we validate the efficiency of GL-SA by comparing the memory consumption with vanilla self-attention during the training process.

Algorithm 1: Grouped Local Self-Attention

Data: Local embedding $L = \{l_i\}_{i=0}^M$, Anchor query
 $Q = \{Q_i\}_{i=0}^{\hat{M}} = \{Cat(P_i, C_i)\}_{i=0}^{\hat{M}}$

Result: Anchor query \hat{Q} for the self-attention computation is completed

1 $q, k \leftarrow \{C_i\}_{i=0}^{\hat{M}} + sinPE(\{P_i\}_{i=0}^{\hat{M}})$; /* $sinPE(\cdot)$: sine positional encoding. */
2 $v \leftarrow \{C_i\}_{i=0}^{\hat{M}}$; /* $v \in \mathbb{R}^{b*(M*N)*d}$ */
3 $L_q, L_p \leftarrow split(L)$; /* $L_q \in \mathbb{R}^{M*b*d}$ */

4 **step1: Local feature extraction**

5 $k_{Q1}, v_{Q1} \leftarrow RLinear(k, v)$; /* $RLinear(\cdot)$: Reconstruct the shape of the output from the linear layer. $k_{Q1}, v_{Q1} \in \mathbb{R}^{(M*b)*N*d}$ */
6 $q_{Lq}, q_{Lp} \leftarrow RLinear(L_q, L_p)$; /* $L_q \in \mathbb{R}^{(M*b)*1*d}$ */
7 $\Psi_q, \Psi_p \leftarrow FInter1((q_{Lq}, q_{Lp}), k_{Q1}, v_{Q1})$; /* $FInter1(\cdot)$: Feature interaction. $\Psi_q, \Psi_p \in \mathbb{R}^{M*b*d}$ */

8 **step2: Feature interaction among groups**

9 $q_m \leftarrow mean(\{C_i\}_{i=0}^{\hat{M}} + sinPE(\{P_i\}_{i=0}^{\hat{M}}))$
10 $\Psi_2 \leftarrow mean(\Psi_p + \Psi_q) + q_m$
11 $\Psi'_2 \leftarrow van.(\Psi_2)$; /* $van.(\cdot)$: vanilla self-attention. */

12 **step3: Feature interaction within groups**

13 $q_{Q2}, k_{Q2}, v_{Q2} \leftarrow RLinear(q, k, v)$; /* $v_{Q2} \in \mathbb{R}^{(M*b)*N*d}$ */
14 $k_{L2}, v_{L2} \leftarrow RLinear(\Psi'_2)$; /* $v_{L2} \in \mathbb{R}^{(M*b)*1*d}$ */
15 $k_{LQ}, v_{LQ} \leftarrow Cat((k_{L2}, k_{Q2}), (v_{L2}, v_{Q2}))$; /* $k_{LQ}, v_{LQ} \in \mathbb{R}^{(M*b)*(N+1)*d}$ */
16 $\hat{Q} \leftarrow FInter2(q_{Q2}, k_{LQ}, v_{LQ})$; /* $FInter2(\cdot)$: Feature interaction. */

17 **return** \hat{Q}

3.4 Matching and Supervise

The structure of EAN-MapNet is divided into a primary part and an auxiliary part, both of which are separately matched and supervised, with the matching and supervision methods inspired by MapTR [10]. Assuming the loss of the primary part is denoted as L_{center} and the loss of the auxiliary part is denoted as $L_{non-center}$, the overall loss is given by Equation(7).

$$L = \lambda_1 L_{center} + \lambda_2 L_{non-center} \quad (7)$$

Referring to [11], we propose EAN-MapNet++, which is based on EAN-MapNet with segmentation-based loss L_{seg} and depth estimation loss L_{depth} . The loss values of EAN-MapNet++ are shown Equation(8).

$$L_{++} = \lambda_1 L_{center} + \lambda_2 L_{non-center} + \lambda_3 L_{seg.} + \lambda_4 L_{depth} \quad (8)$$

For BEV feature, $L_{seg.}$ loss reinforces the feature representation of map elements regions, while L_{depth} strengthens the representation of depth information.

4 Experiments

4.1 Dataset and Metric

We evaluate the performance of the EAN-MapNet using the nuScenes dataset [28]. The model is trained with images captured by 6 surround-view cameras. The predicted HD map range within a single frame is $[-15m, 15m]$ along the X-axis and $[-30m, 30m]$ along the Y-axis in the ego-vehicle coordinate system. And the categories of the predicted map elements include pedestrian crossing, lane divider and boundary.

We matched the predicted and GT using three thresholds of Chamfer distance $\tau = 0.5, 1.0, 1.5$, and subsequently calculated the map construction quality AP_τ for each threshold. Then the average AP of $\{AP_\tau\}_{\tau}^{\{0.5,1.0,1.5\}}$ is then used as a criterion for model model performance evaluation.

4.2 Implementation Details

EAN-MapNet uses GKT [29] to generate BEV feature, while EAN-MapNet++ selects LSS [30] as the BEV generation network to ensure a fair comparison with MapTRv2. The optimizer uses AdamW and the initial learning rate is set to 2.5×10^{-4} . The default training schedule is 24 epochs and the batch size is 4.

In ablation study 4.4 (1) and (2), the grouping number of initial query units is set to 50, and we utilize 1 NVIDIA A40 with the weight decay is 0.01. For all other conditions, the grouping number of initial query units is set to 100, and experiments are conducted using 1 NVIDIA GeForce RTX 3090 with the weight decay is 1.25×10^{-3} .

In the loss function, $\lambda_0 = \lambda_1 = \lambda_2 = \lambda_3 = 1$; for the neighborhood configuration, when local queries are not improved, $\omega = 0.25$ and $a = 0.55m$; otherwise, $\omega = 0.2$ and $a = 0.5m$.

4.3 Comparisons with state-of-the-art methods

As shown in [Table\(1\)](#), we compare EAN-MapNet with state-of-the-art methods. All methods take images as input, with image size set to (480, 800), and a batch size of 4 is employed during training.

Compared to MapTR [10], EAN-MapNet demonstrates a significant improvement of 9.4 mAP in prediction accuracy. Additionally, despite doubling the number of initial queries in EAN-MapNet compared to MapTR, the inference speed only decreases by 2.2 fps. Furthermore, with identical segmentation loss supervision and depth estimation supervision, EAN-MapNet++ enhances prediction accuracy by 1.5 mAP compared to MapTRv2 [11], while also reducing memory consumption by 8198M during training. Additionally, EAN-MapNet outperforms PivotNet [33] by 2.6 mAP. Compared to BeMapNet, EAN-MapNet++ significantly surpasses BeMapNet [32], with a margin of 3.2 mAP. Simultaneously, we performed qualitative visualization in [Fig\(6\)](#).

Table 1: Comparisons with SOTAs. “-” represents that the result is not available. For fairness, we tested the FPS on an RTX 3090, maintaining consistent input image shapes of (480, 800) and a batch size of 4 for memory consumption testing.

Method	Epoch	AP↑				FPS ↑	GPU mem. ↓
		ped.	div.	bou.	mean		
VectorMapNet [31]	110	36.1	47.3	39.3	40.9	1.5	20237M
BeMapNet [32]	30	57.7	62.3	59.4	59.8	-	-
PivotNet [33]	24	56.2	56.5	60.1	57.6	-	-
MapTR [10]	24	46.3	51.5	53.1	50.3	17.2	10152M
GAN-MapNet	24	55.9	61.7	61.5	59.7	14.9	10838M
MapTRv2 [11]	24	59.8	62.4	62.4	61.5	13.3	19299M
GAN-MapNet++	24	60.5	62.1	66.3	63.0	12.6	11101M

Table 2: Effectiveness of Grouped Local Self-Attention with anchor queries.

	mAP	GPU mem.	FPS
vanilla queries	52.4	10152M	17.2
anchor queries	54.6	10235M	17.0
GL-SA	54.9	8022M	15.5

Table 3: Effectiveness of each module in Grouped Local Self-Attention, \mathbb{L} denotes the local queries, and \mathbb{M} represents the mean of anchor queries.

	\mathbb{L}	\mathbb{M}	mAP	GPU mem.
	✗	✗	53.0	7922M
	✓	✗	53.9	8022M
	✓	✓	54.9	8022M

4.4 Ablation Study

(1) Effectiveness of GL-SA with anchor queries: As shown in Table(2), compared to using vanilla queries, our defined anchor queries improve prediction accuracy by 2.3 mAP. Subsequently, After incorporating the use of GL-SA on top of setting anchor queries, there is a reduction in memory consumption by 2213M, with a corresponding improvement in prediction accuracy of 0.3mAP.

(2) Effectiveness of each module in GL-SA: As shown in Table(3), we observe that the introduction of local queries increases memory consumption by only 100 M, while improving prediction accuracy by 1.9 mAP. Additionally, the strengthening effect of \mathbb{M} is evident, resulting in a 1.0 mAP increase in prediction accuracy without any additional memory overhead.

(3) Effectiveness of the anchor neighborhoods: We conducted four sets of experiments: (a) baseline, (b) introducing anchor neighborhoods on top of (a),

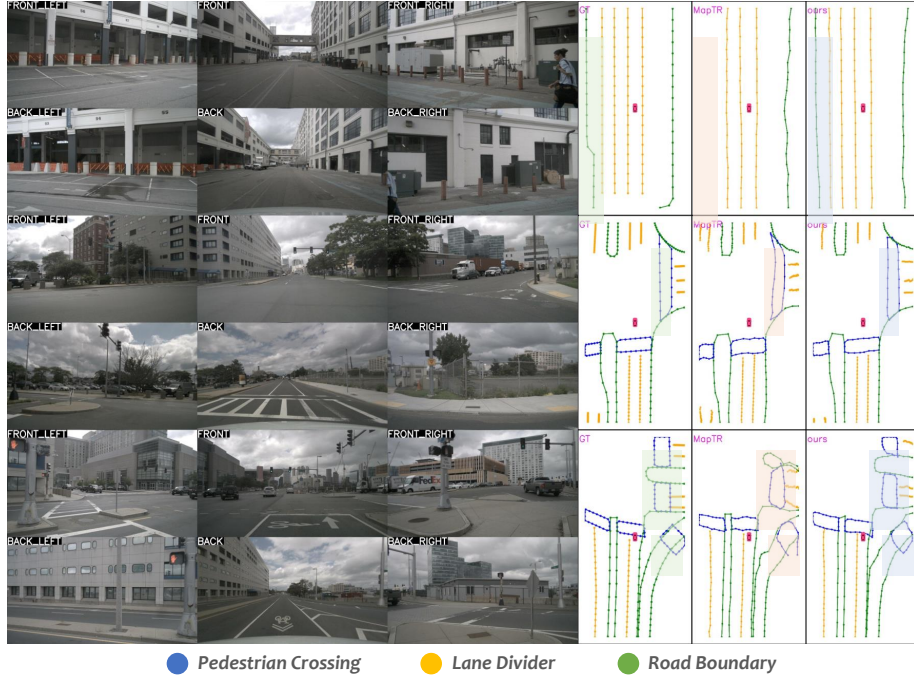


Fig. 6: Comparison with baseline on qualitative visualization. The visualizations demonstrate the superiority and robustness of EAN-MapNet in the task of detecting map elements.

(c) introducing GT neighborhoods on top of (b), and (d) utilizing improved local queries on top of (c). The results are shown in Table(4).

Comparing (a) and (b), the use of anchor neighborhoods only increased by 0.5 mAP. This is because there is conflict and ambiguity when both neighborhood central anchors and non-neighborhood central anchors are fitted to the same target points through the shared content parts. Therefore, with the introduction of GT neighborhoods in (c), the prediction accuracy of the network significantly improved by 2.5 mAP. Furthermore, comparing (d) with (c), the prediction accuracy increased by 1.0 mAP, indicating that the improved structure of the local queries can significantly enhance the ability to aggregate local feature.

(4) Additional evidence confirming the effectiveness of anchor neighborhoods: As shown in Table(5), when the positions of the non-neighborhood central anchors are not constrained by the anchor neighborhoods but are randomly distributed on the BEV plane, the experimental result is 1.4 mAP higher than that of "anchor neighborhoods" without the introduction of GT neighborhoods. However, with the introduction of GT neighborhoods to alleviate fitting ambiguities, "anchor neighborhoods" surpasses "random anchors" by 0.8 mAP. This suggests that when the non-neighborhood central anchors are within the an-

chor neighborhoods, they exhibit stronger positional correlation with the neighborhood central anchors, thereby better assisting in fitting the neighborhood central anchors to the target points.

Table 4: Effectiveness of the anchor neighborhoods.

Index	Method	mAP
(a)	baseline	56.2
(b)	(a) + anchor neighborhoods	56.7
(c)	(b) + GT neighborhoods	58.7
(d)	(c) + improved local queries	59.7

Table 5: Effectiveness of the anchor neighborhoods. When non-neighborhood central anchors are within the neighborhoods, labeled as "anchor neighborhoods", and without restrictions on their neighborhoods, labeled as "random anchors".

	GT neighborhoods	mAP
anchor neighborhoods	✗	56.7
	✓	58.7
random anchors	✗	58.1
	✓	57.9

5 Conclusions

In this paper, we propose EAN-MapNet, which integrates the physical location features of anchor neighborhoods into its initial query units. Additionally, we propose GL-SA, which efficiently and comprehensively achieves feature interaction among anchor queries. On the nuScenes dataset, we validate the effectiveness of anchor neighborhoods design, whereby non-neighborhood central anchors effectively assist neighborhood central anchors in fitting to target points, significantly improving prediction accuracy. Regarding GL-SA, experiments demonstrate its ability to facilitate more effective feature interaction among queries while greatly reducing computational complexity. Additionally, through comparisons with other works, EAN-MapNet achieves a state-of-the-art performance.

References

1. Mayank Bansal, Alex Krizhevsky, and Abhijit Ogale. Chauffeurnet: Learning to drive by imitating the best and synthesizing the worst. *arXiv preprint arXiv:1812.03079*, 2018.
2. Henggang Cui, Vladan Radosavljevic, Fang-Chieh Chou, Tsung-Han Lin, Thi Nguyen, Tzu-Kuo Huang, Jeff Schneider, and Nemanja Djuric. Multimodal trajectory predictions for autonomous driving using deep convolutional networks. In *2019 International Conference on Robotics and Automation (ICRA)*, pages 2090–2096. IEEE, 2019.
3. Yuning Chai, Benjamin Sapp, Mayank Bansal, and Dragomir Anguelov. Multipath: Multiple probabilistic anchor trajectory hypotheses for behavior prediction. *arXiv preprint arXiv:1910.05449*, 2019.
4. Huiyuan Xiong, Taohong Zhu, Yu Liu, Yuelong Pan, Shaofang Wu, and Long Chen. Road-model-based road boundary extraction for high definition map via lidar. *IEEE Transactions on Intelligent Transportation Systems*, 23(10):18456–18465, 2022.
5. Ji Zhang and Sanjiv Singh. Loam: Lidar odometry and mapping in real-time. In *Robotics: Science and systems*, volume 2, pages 1–9. Berkeley, CA, 2014.
6. Raul Mur-Artal and Juan D Tardós. Orb-slam2: An open-source slam system for monocular, stereo, and rgbd cameras. *IEEE transactions on robotics*, 33(5):1255–1262, 2017.
7. Qi Li, Yue Wang, Yilun Wang, and Hang Zhao. Hdmapnet: An online hd map construction and evaluation framework. In *2022 International Conference on Robotics and Automation (ICRA)*, pages 4628–4634. IEEE, 2022.
8. Hao Dong, Xianjing Zhang, Jintao Xu, Rui Ai, Weihao Gu, Huimin Lu, Juho Kannala, and Xieyuanli Chen. Superfusion: Multilevel lidar-camera fusion for long-range hd map generation. *arXiv preprint arXiv:2211.15656*, 2022.
9. Lang Peng, Zhirong Chen, Zhangjie Fu, Pengpeng Liang, and Erkang Cheng. Bevsegformer: Bird’s eye view semantic segmentation from arbitrary camera rigs. In *Proceedings of the IEEE/CVF Winter Conference on Applications of Computer Vision*, pages 5935–5943, 2023.
10. Bencheng Liao, Shaoyu Chen, Xinggang Wang, Tianheng Cheng, Qian Zhang, Wenyu Liu, and Chang Huang. Maptr: Structured modeling and learning for online vectorized hd map construction. *arXiv preprint arXiv:2208.14437*, 2022.
11. Bencheng Liao, Shaoyu Chen, Yunchi Zhang, Bo Jiang, Qian Zhang, Wenyu Liu, Chang Huang, and Xinggang Wang. Maptrv2: An end-to-end framework for online vectorized hd map construction. *arXiv preprint arXiv:2308.05736*, 2023.
12. Tianyuan Yuan, Yicheng Liu, Yue Wang, Yilun Wang, and Hang Zhao. Streammapnet: Streaming mapping network for vectorized online hd map construction. In *Proceedings of the IEEE/CVF Winter Conference on Applications of Computer Vision*, pages 7356–7365, 2024.
13. Zhenhua Xu, Kenneth KY Wong, and Hengshuang Zhao. Insightmapper: A closer look at inner-instance information for vectorized high-definition mapping. *arXiv preprint arXiv:2308.08543*, 2023.
14. Jingyi Yu, Zizhao Zhang, Shengfu Xia, and Jizhang Sang. Scalablemap: Scalable map learning for online long-range vectorized hd map construction. *arXiv preprint arXiv:2310.13378*, 2023.
15. Nicolas Carion, Francisco Massa, Gabriel Synnaeve, Nicolas Usunier, Alexander Kirillov, and Sergey Zagoruyko. End-to-end object detection with transformers. In *European conference on computer vision*, pages 213–229. Springer, 2020.

16. Xizhou Zhu, Weijie Su, Lewei Lu, Bin Li, Xiaogang Wang, and Jifeng Dai. Deformable detr: Deformable transformers for end-to-end object detection. *arXiv preprint arXiv:2010.04159*, 2020.
17. Feng Li, Hao Zhang, Shilong Liu, Jian Guo, Lionel M Ni, and Lei Zhang. Dn-detr: Accelerate detr training by introducing query denoising. In *Proceedings of the IEEE/CVF Conference on Computer Vision and Pattern Recognition*, pages 13619–13627, 2022.
18. Hao Zhang, Feng Li, Shilong Liu, Lei Zhang, Hang Su, Jun Zhu, Lionel M Ni, and Heung-Yeung Shum. Dino: Detr with improved denoising anchor boxes for end-to-end object detection. *arXiv preprint arXiv:2203.03605*, 2022.
19. Yingming Wang, Xiangyu Zhang, Tong Yang, and Jian Sun. Anchor detr: Query design for transformer-based object detection. *arXiv preprint arXiv:2109.07107*, 3(6), 2021.
20. Depu Meng, Xiaokang Chen, Zejia Fan, Gang Zeng, Houqiang Li, Yuhui Yuan, Lei Sun, and Jingdong Wang. Conditional detr for fast training convergence. In *Proceedings of the IEEE/CVF International Conference on Computer Vision*, pages 3651–3660, 2021.
21. Shilong Liu, Feng Li, Hao Zhang, Xiao Yang, Xianbiao Qi, Hang Su, Jun Zhu, and Lei Zhang. Dab-detr: Dynamic anchor boxes are better queries for detr. *arXiv preprint arXiv:2201.12329*, 2022.
22. Ashish Vaswani, Noam Shazeer, Niki Parmar, Jakob Uszkoreit, Llion Jones, Aidan N Gomez, Łukasz Kaiser, and Illia Polosukhin. Attention is all you need. *Advances in neural information processing systems*, 30, 2017.
23. Noam Shazeer. Fast transformer decoding: One write-head is all you need. *arXiv preprint arXiv:1911.02150*, 2019.
24. Joshua Ainslie, James Lee-Thorp, Michiel de Jong, Yury Zemlyanskiy, Federico Lebrón, and Sumit Sanghai. Gqa: Training generalized multi-query transformer models from multi-head checkpoints. *arXiv preprint arXiv:2305.13245*, 2023.
25. Haoyi Zhou, Shanghang Zhang, Jieqi Peng, Shuai Zhang, Jianxin Li, Hui Xiong, and Wancai Zhang. Informer: Beyond efficient transformer for long sequence time-series forecasting. In *Proceedings of the AAAI conference on artificial intelligence*, volume 35, pages 11106–11115, 2021.
26. Wenjie Gao, Jiawei Fu, Haodong Jing, and Nanning Zheng. Complementing on-board sensors with satellite map: A new perspective for hd map construction. *arXiv preprint arXiv:2308.15427*, 2023.
27. Ziyang Xie, Ziqi Pang, and Yu-Xiong Wang. Mv-map: Offboard hd-map generation with multi-view consistency. In *Proceedings of the IEEE/CVF International Conference on Computer Vision*, pages 8658–8668, 2023.
28. Holger Caesar, Varun Bankiti, Alex H Lang, Sourabh Vora, Venice Erin Liong, Qiang Xu, Anush Krishnan, Yu Pan, Giancarlo Baldan, and Oscar Beijbom. nuscenes: A multimodal dataset for autonomous driving. In *Proceedings of the IEEE/CVF conference on computer vision and pattern recognition*, pages 11621–11631, 2020.
29. Shaoyu Chen, Tianheng Cheng, Xinggang Wang, Wenming Meng, Qian Zhang, and Wenyu Liu. Efficient and robust 2d-to-bev representation learning via geometry-guided kernel transformer. *arXiv preprint arXiv:2206.04584*, 2022.
30. Jonah Philion and Sanja Fidler. Lift, splat, shoot: Encoding images from arbitrary camera rigs by implicitly unprojecting to 3d. In *Computer Vision–ECCV 2020: 16th European Conference, Glasgow, UK, August 23–28, 2020, Proceedings, Part XIV 16*, pages 194–210. Springer, 2020.

31. Yicheng Liu, Tianyuan Yuan, Yue Wang, Yilun Wang, and Hang Zhao. Vectormapnet: End-to-end vectorized hd map learning. In *International Conference on Machine Learning*, pages 22352–22369. PMLR, 2023.
32. Limeng Qiao, Wenjie Ding, Xi Qiu, and Chi Zhang. End-to-end vectorized hd-map construction with piecewise bezier curve. In *Proceedings of the IEEE/CVF Conference on Computer Vision and Pattern Recognition*, pages 13218–13228, 2023.
33. Wenjie Ding, Limeng Qiao, Xi Qiu, and Chi Zhang. Pivotnet: Vectorized pivot learning for end-to-end hd map construction. In *Proceedings of the IEEE/CVF International Conference on Computer Vision*, pages 3672–3682, 2023.